Forging and Heat Treatment Conditions That Produce Visible Grains in a Nickel Alloy

M.C. Hardy[1*], R.C. Buckingham[1], K. Severs[2], B. Cockings[3], J. McCarley[4], K. Ho[4], C. Argyrakis[1] and S. Tin[5]

[1]Rolls-Royce plc, PO Box 31, Derby, DE24 8BF, UK.
[2]ATI Forged Products Cudahy, 5481 S. Packard Avenue, Wisconsin 53110, USA.
[3]Institute of Structural Materials, Swansea University, Fabian Way, Swansea SA1 8EN, UK
[4]Mechanical, Materials and Aerospace Engineering Department, Illinois Institute of Technology, 10 West 32nd Street, Chicago, Illinois 60616, USA.
[5]Department of Materials Science and Engineering, University of Arizona, 1235 E. James E. Rogers Way, Tucson, Arizona 85721, USA.

Abstract

Experiments were undertaken to understand forging and heat treatment conditions that give rise to large, visible grains in a new nickel alloy after super-solvus heat treatment. Such grains are undesirable as they reduce strength and low cycle fatigue performance. The information that is reported is required to design a forging practice to manufacture closed die forgings, intended for disk rotors that are used in gas turbine engines. The alloy is a development composition, which contains about 51 % gamma prime and has been produced by powder metallurgy. Compression tests were conducted to specified upsets on right circular cylinder and double cone test pieces. Segments of double cones were heat treated and examined to characterise grain size. The results of these experiments are understood having reviewed starting microstructure, the results of process simulations, and the results of electron backscattered diffraction on forged material.

Introduction

High bypass ratio turbofan aircraft engines and operating cycles are continuously evolving to provide improved efficiencies for reduced fuel consumption and emissions [1, 2]. However, whilst propulsive and aerodynamic optimizations of aircraft engines are possible, the increased demands upon superalloys, which are used in the hot section parts, limit the thermal efficiency improvements that can be achieved. The requirements for reduced engine core sizes and increased temperatures and stresses pose a complex set of seemingly conflicting property requirements for the materials considered for safety-critical disk rotor applications. Specifically, materials with higher strength levels are needed to reduce the size and weight of components. Whilst this necessitates the development of compositions with increased amounts of the gamma prime (γ') phase, further optimization is possible by using a fine grain size. Yet such grain structures produce less appealing time dependent crack growth behaviour [4], which may limit the design life of the component or the interval between inspections. This is more relevant in today's engines as high climb rates are increasingly required by commercial airlines to move aircraft more quickly to altitude to reduce fuel burn [5]. Therefore, acceptable strength is required from coarse grain microstructures, which demands effective precipitation strengthening from alloy design [6] and control of grain size in near net shaped forgings.

* corresponding author, mark.hardy@rolls-royce.com

Inevitably, this is only possible using powder metallurgy to minimize elemental segregation to length scales of a micron (µm) or less for these complex, multi-component alloys with high levels of reactive elements (Al, Ti, Ta *etc.*) [7-9]. Subsequent hot deformation of consolidated powder compacts produces billet material with extremely fine grains, which enables superplastic flow of the work piece during isothermal forging at high temperatures and low strain rates, to make the desired near net disc shapes [7-9]. A uniform average grain size of 20-40 µm can then be created by super-solvus solution heat treatment. This microstructure produces an ideal balance in material properties between tensile strength and resistance to time dependent crack growth.

Closed die forgings, from which disc rotors are produced, often show significant variations in forging strain due to changes in geometry, notably for drive arms. Factors that control grain size in these large complex forgings, after solution heat treatment above the γ' solvus temperature (T_{solvus}), have been discussed by the authors in an earlier publication [10]. These include, (i) the size of grains and γ' microstructure in the billet material or forging stock, (ii) forging temperatures and strain rates that promote super plastic forming, (iii) the effects of low forging strains and relevant strain rates for isothermal forgings, (iv) heating rates employed for solution heat treatment, (v) the role of grain boundary primary γ' precipitates and other pinning particles such as primary MC carbides. This understanding has guided the compression testing and heat treatment experiments that are reported in this paper.

The earlier publication also discussed studies in which electron backscattered diffraction (EBSD) has been used to understand the mechanisms that give rise to visible grains. Bozzolo *et al.* [11, 12] observed that large visible grains have low values of stored energy and concluded that stored energy is the driving force for overcoming the Smith-Zener pinning pressure that is provided by pinning particles such as primary γ'. It was proposed that selective grain growth is due to the activation of a few nuclei (from low forging strains) that have sufficient stored energy to exceed a critical value, which appears to decrease with increasing heating time for super-solvus solution heat treatment. This suggests that the observed behaviour is a recrystallisation phenomenon that requires a critical strain or stored energy. Miller *et al.* [13] have also shown that the low grain growth front velocities, less than 1 µm per s, that have been cited for abnormal grain growth in other alloys, were not found in René 88DT. Much higher values were reported, suggesting that the critical process is not abnormal grain growth but abnormal recrystallization with a low density of nuclei.

Table 1 Alloy composition [14].

wt.%	Ni	Co	Cr	Fe	Mn	Mo	W	Al	Ti	Ta	Nb	Si	C	B	Zr	Hf
min	Bal.	14.6	11.5	0.8	0.2	2.0	3.3	2.9	2.6	3.6	1.2	0.1	0.02	0.01	0.05	0.000
max	Bal.	15.9	13.0	1.2	0.6	2.4	3.7	3.3	3.1	5.1	1.8	0.6	0.06	0.03	0.11	0.045

Initial microstructure

Compression tests were undertaken on a new alloy composition (Table 1), which has been specified in [14] and reported in [6]. Differential scanning calorimetry and metallographic examination of small samples, heated using rates of at least 10°C/min., indicate that the alloy T_{solvus} is about 1160 to

1165°C. Two batches of starting material have been considered in this study. In Table 2, these are referred to as Microstructure 1 and 2. Both batches were produced from argon gas atomised powder that had been screened to -270 mesh (53 µm), consolidated by hot isostatic pressure, and then subjected to hot deformation.

Table 2 Microstructure and test piece details. The grain size ratings were established from optical microscopy, with samples etched using Kalling's Reagent. RCC refers to right circular cylinder test pieces.

Microstructure	Grain size ASTM E112	RCC dims. (mm)	Soak time
1	90 % ASTM 15, 10 % 8.5 - 9, ALA 6.5 - 6	ϕ10 x 13.3 high	4 or 8 h
2	more than 99.9 % less than ASTM 12	ϕ12 x 16 high	15-30 mins

Images of samples from Microstructure 2 are shown in Fig. 1. The inverse pole figure (IPF) image, from electron backscattered diffraction (EBSD), provides better resolution than those of etched samples from optical microscopy, from which the grain size ratings in Table 2 were derived. The step size used for EBSD was 0.3 µm and the area examined was 250 x 250 µm. Note that EBSD does not differentiate gamma (γ) grains from primary γ' precipitates. There is a large volume fraction of primary γ' precipitates in the starting material of the development alloy, about 32-37% in the optical microscope image in Fig. 1 (right). These are the white particles in the sample, which was electrolytically etched with 10% phosphoric acid (H_3PO_4) solution. When expressed as an equivalent circular diameter, primary γ' precipitates are typically 1 – 2 µm in size. The larger γ grains in the IPF image, Fig. 1 (left), show twins from hot deformation and appear to be greater than ASTM 12 (5.6 µm). A Kernel Average Misorientation (KAM) image, calculated from EBSD data, is also provided in Fig. 1 (centre). This is the average misorientation between a point and its nearest neighbours and is a useful measure of retained strain, as shown by the bright green areas in the KAM image that are for rotations of 5°. These bright green locations are often at the interface between γ grains or the interface between γ grains and primary γ' particles.

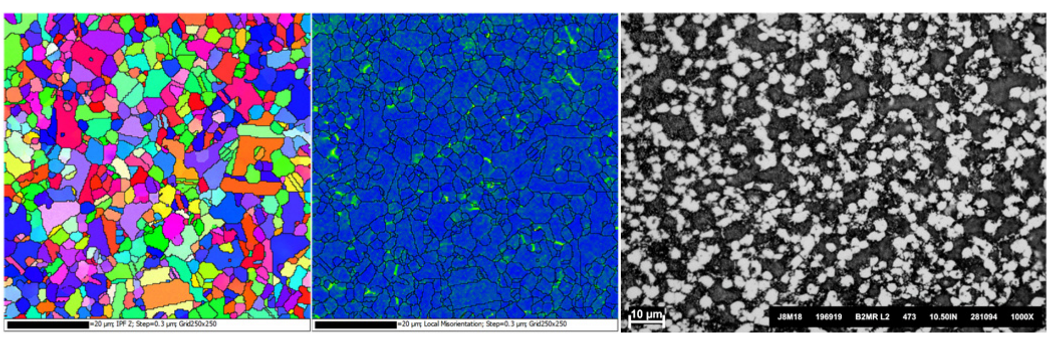

Fig. 1 Images of Microstructure #2, from electron backscatter diffraction (EBSD), (left) inverse pole figure (IPF), (centre) kernal average misorientation (KAM), with green indicating 5° rotations. Optical micrograph (right) shows primary γ' precipitates (white), electrolytically etched with 10 % H_3PO_4 solution. Circa 32-37 % primary γ' precipitates.

Experimental Work

Initially isothermal compression tests were conducted on right circular cylinder (RCC) test pieces, for Microstructure 1, at Swansea University to understand the effect of forging conditions (temperatures of 1050, 1075, 1100 and 1125°C and strain rates of 0.1, 0.01 and 0.001 strain per s) on flow stress. They were conducted under constant strain rate control using a servo-hydraulic test frame fitted with Mar-M002 flat die platens. A split box resistive elements furnace placed around the platens provided a temperature capability of up to 1200°C where temperature control was provided by two N-type thermocouples attached to the bottom platen. Temperature control was specified to be within ±3°C of the target test temperature. All test pieces were given a single coat of boron nitride prior to upset to minimise friction effects and inhibit the test piece from sticking to the platens on compression. Test pieces were pre-soaked to either 4 or 8 hours, as indicated in Table 2. Test pieces were pre-soaked using a bench-top resistive elements furnace for a period of 3.5 and 7.5 hours with the final 30 minutes being applied on the test frame prior to upset. Raw data was provided in the form of platen position (in mm) versus load (in kN), from which the true stress and true strain values were calculated. Friction and adiabatic heating effects were considered during data analysis using software proprietary to Swansea University.

Isothermal compression tests for Microstructure 2 were conducted on RCC test pieces (Table 2) at the Illinois Institute of Technology at a constant strain rate of 0.2 strain per min. (about 0.003 strain per s) using a servo-hydraulic test frame and loading bars fitted with Si_3N_4 anvils. Temperature control was provided by K-type thermocouples, which were attached to test pieces. Boron nitride coating was applied to both test pieces and anvils. Unlike the test pieces from Microstructure 1, test pieces from Microstructure 2 were not soaked for 4 or 8 hours at the forging temperature prior to compression testing. This was an error and not intentional. As such, differences in flow stress behaviour between Microstructures 1 and 2 were expected due to differences in starting grain size (Table 2) and secondary γ' % and size.

To understand the effect of forging conditions on grain size, isothermal compression tests were conducted on 2-inch (Microstructure 1) and 2.5-inch (Microstructure 2) double cone (DC) test pieces (Fig. 2) at ATI Forged Products, Cudahy using a laboratory isothermal press. Test pieces were soaked for 8 hours at the forging temperature prior to upset or loss of height of about 50%. Forging temperatures of 1050, 1075, 1100 and 1125°C were examined for Microstructure 1, with a constant strain rate of 0.2 per minute. The results of work on Microstructure 1 informed the subsequent tests on Microstructure 2, which were undertaken at forging temperatures of 1030, 1045, 1060 and 1075°C. In addition to a strain rate of 0.2 strain per min., DC test pieces from Microstructure 2 were also forged at 0.05 and 0.5 strain per min. at 1060°C. After forging, DC test pieces were cut into quarters for solution heat treatment. To simulate large forgings, the DC quarters were subjected to the following heating profile to a solution heat treatment (SHT) temperature of 1185°C: 900 to 1115°C at a rate of 10°C/min., 1115 to 1155°C at 4°C/min., 1155 to 1175°C at 1°C/min. and 1175 to 1185°C at 0.5°C/min. On reaching 1185°C, they were soaked for 1 hour.

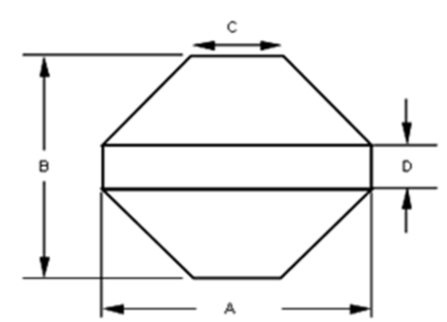

Fig. 2 Sketch of a double cone (DC) compression test piece. For 2-inch DC test pieces, A = 50.8 mm, B = 42.2 mm, C = 17 mm and D = 8.4 mm. For 2.5-inch DC test pieces, A = 63.5 mm, B = 52.75 mm, C = 21.25 mm and D = 10.5 mm.

Grain size in the DC quarters was assessed from back scattered electron (BSE) images of polished surfaces, either visually to confirm the presence of large visible grains or to determine mean grain size using lineal intercept method, according to ASTM E112.

To complement DC experiments, samples were cut from a 12 mm diameter bar, which was wire electro-discharge machined from the centre section (55 mm in diameter x 151 mm high) of a large forging, produced from Microstructure 2 (Fig. 3). A fraction of each sample was cut for heat treatment trials. The aim was to examine the effect of heating rate on grain size. Four heating rates were considered from 1000°C to the solution heat treatment temperature of 1185°C: 60°C/min. (duration of about 3 mins.), 5°C/min. (duration of about 37 mins.), 2.1°C/min. (duration of about 88 mins.) and 1.3°C/min. (duration of about 142 mins.). Samples were soaked for 1 hour at 1185°C and then air cooled. Grain size was rated according to ASTM E112 and E930 from optical microscope images of surfaces etched with Kalling's Reagent. Polished surfaces were also assessed using EBSD.

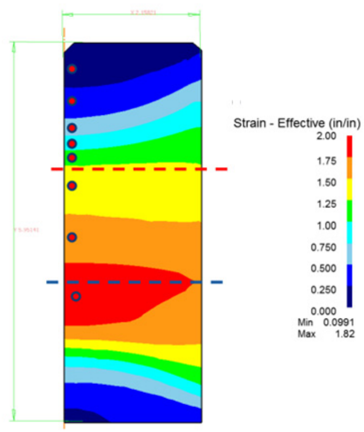

Fig. 3 Half section of a forging bore centre (55 mm in diameter x 151 mm) showing the location of samples taken from a 12 mm diameter bar. The coloured contours indicate effective strain values from a DEFORM forging simulation.

Process Models

Forging simulations were undertaken using commercial finite element package DEFORM®. Half of the model domain was created using axisymmetric elements with automatic remeshing and increased size control at highly curved locations. An optimised Coulomb friction coefficient of 0.07 was used after correlating the final workpiece geometry with the deformed model geometry. The simulation was stopped once a 50 % reduction in original height was achieved. Contour plots of effective strain and maximum instantaneous strain rate (at the end of the forging step) were extracted and are presented in this paper. The die or crosshead speed was set to reduce logarithmically versus the die displacement to simulate as close as possible constant strain rate conditions.

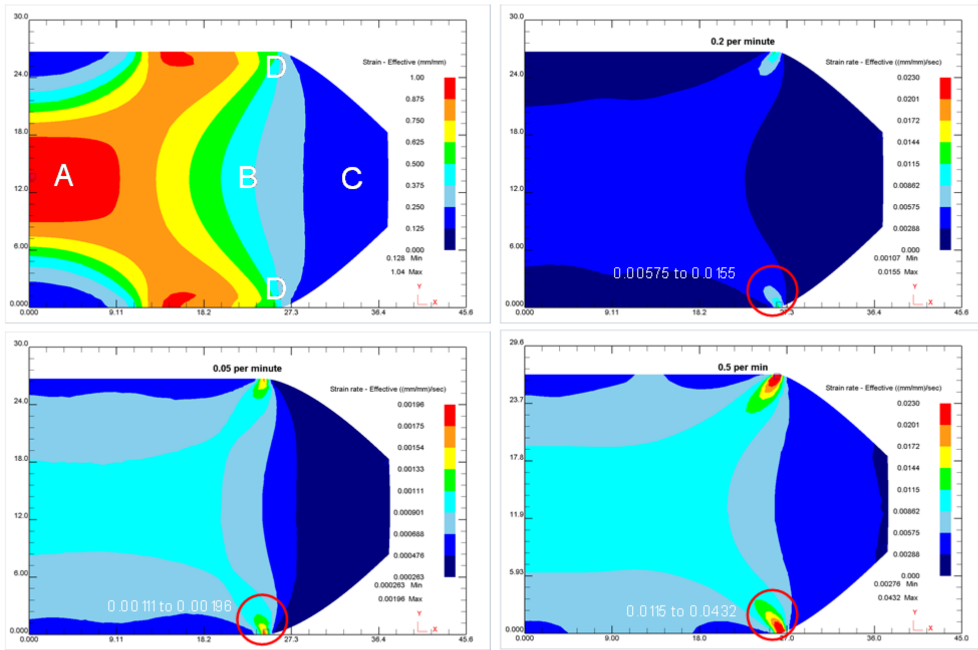

Fig. 4 Results of DEFORM forging simulations on the 2-inch double cone test piece after 50% reduction in height. Top left image shows predicted effective strain contours, noting locations A, B, C and D. The other 3 images show predicted maximum instantaneous strain contours values for a double cone forged at 0.2 per min. (top left), 0.05 per min. (lower left) and 0.5 per min. (lower right).

Results from Experimental Work

(i) Flow stress data

An example of the true stress versus true strain data from compression tests on Microstructure 1 is presented in Fig. 5. As expected, the lower strain rates of 0.01 and 0.001 per s produced lower true stress values, which did not change significantly with increasing true strain unlike the true stress values for 0.1 per s that diminished after a strain of 0.1, suggesting grain refinement through dynamic recrystallisation (DRX). Figure 6 shows the influence of temperature on flow stress data for Microstructure 2. The true stress, true strain data follow the expected behaviour, with less change in true stress with increasing true strain for the higher forging temperatures. Forging at 1090°C is associated with a low peak stress value, which changed very little with increasing strain. Considerably higher flow stresses were recorded at forging temperatures of, or below, 1060°C; the flow stress behaviour is similar to that shown in Fig. 5 for high strain rates, in which true stress continues to diminish with increasing true strain, which is indicative of DRX.

Figure 7 correlates peak true stress data with strain rate for both Microstructure 1 and 2. For most test conditions, there is little difference in peak true stresses for Microstructure 1 material that was soaked for 4 or 8 hours; the variation in data for 1050°C/0.1 per s and 1100°C/0.001 per s is likely to be test-to-test scatter. Whilst direct comparisons are not possible, except for 1075°C, peak stress values for unsoaked Microstructure 2 are consistently higher than those for Microstructure 1 despite the greater fraction of coarse grains (Table 2), which is expected to increase flow stress at these forging temperatures.

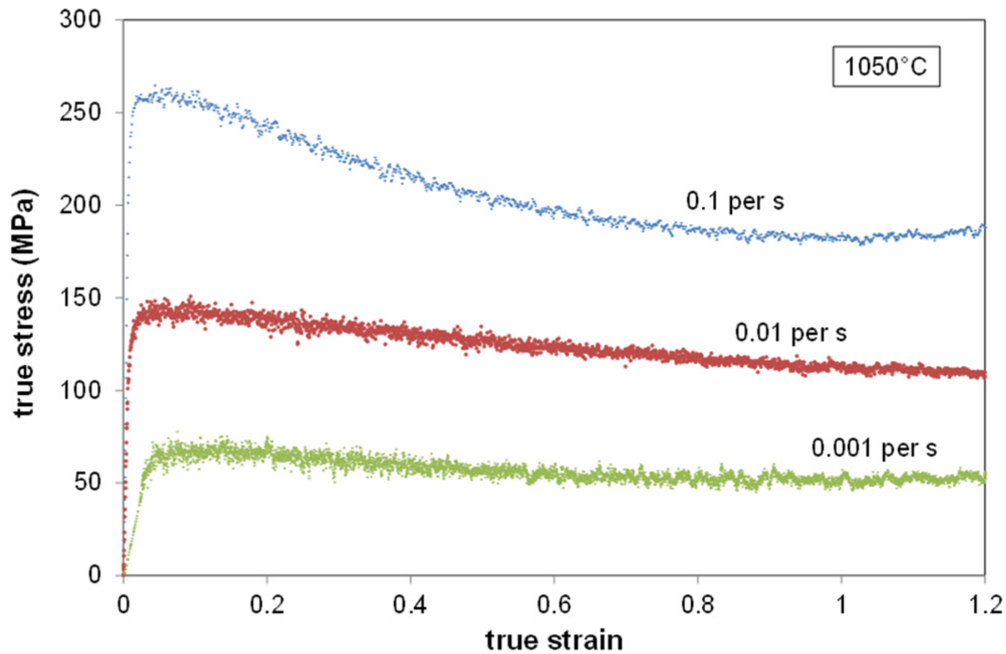

Fig. 5 True stress, true strain data from compression tests on RCC test pieces for Microstructure 1 at 1050°C and strain rates of 0.1, 0.01 and 0.001 strain per s. Test pieces were soaked for 8 hours.

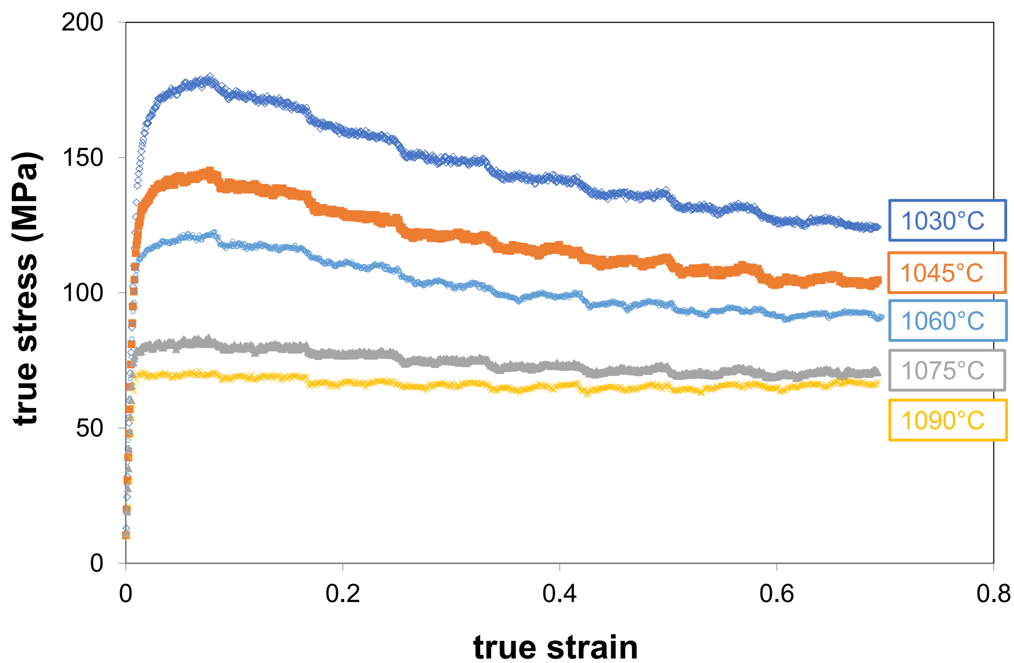

Fig. 6 True stress, true strain data from compression tests on RCC test pieces for Microstructure 2 at a strain rate of 0.2 strain per min. and temperatures of 1030, 1045, 1060, 1075 and 1090°C. test pieces were soak for 15 minutes.

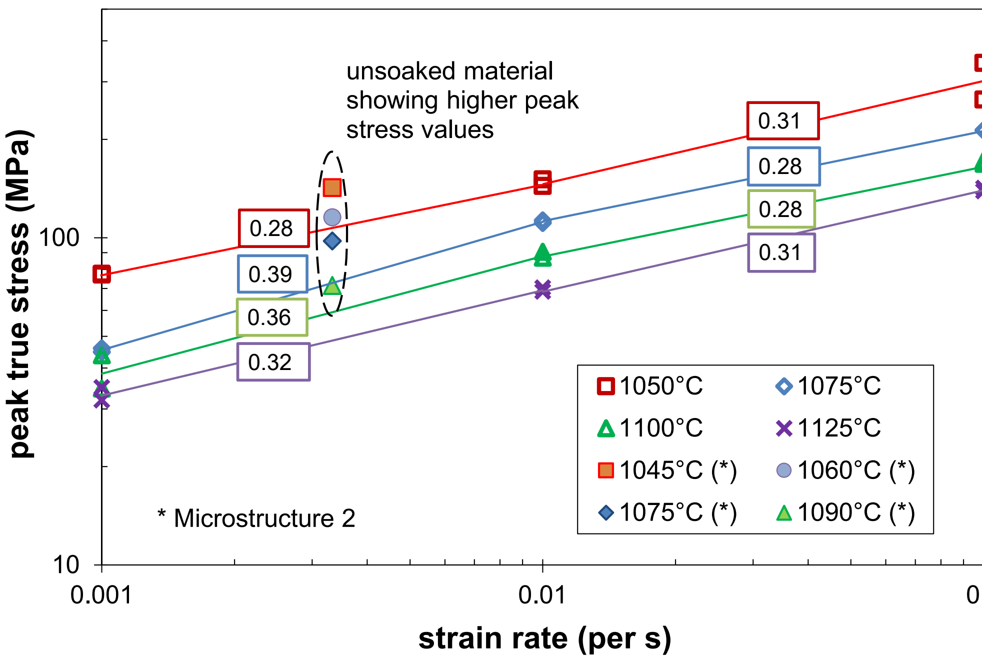

Fig. 7 Peak true stress versus strain rate data for Microstructure 1 (1050, 1075, 1100 & 1125°C) and Microstructure 2 (1045, 1060, 1075 & 1090°C) showing strain rate sensitivity index m values (text in coloured boxes). Straight lines connect data from Microstructure 1 test pieces, which were soaked for 4 and 8 hours.

The strain rate sensitivity index m for describing the power law dependence of flow stress (σ) on strain rate (dε/dt) is from

$$\sigma = K\left(\frac{d\varepsilon}{dt}\right)^{m} \quad [1]$$

where K is a material constant [15]. As the graph axes in Fig. 7 show the logarithm of peak true stress and strain rate, values of m can be determined from the gradients of straight lines that are fitted between data points. These are between 0.28 and 0.39, and are within 0.3 and 0.5, which indicates superplastic deformation.

Table 3 A summary of grain size in forged Microstructure 1 material after solution heat treatment (SHT) at 1185°C for 1 hour. See Fig. 4 for locations A, B and C.

Forge T (°C)	**Mean grain size (µm)**			**ALA grain size (µm)**	**Location**
	A	**B**	**C**		
1125	69	53	74	444	B
1100	26	39	29	306	B/C
1075	26	24	33	107	C
1050	25	29	31	127	B/C

(ii) Grain size

The results of the solution heat treat experiments on forged Microstructure 1 material are summarised in Table 3 for locations A, B and C from quarters of double cone test pieces. It is evident that the ideal mean grain size of 20 – 40 µm grain size was achieved for forging temperatures of 1050, 1075 and 1100°C but not at 1125°C. Since the As Large As (ALA) grains were smaller in material forged at 1050 and 1075°C than at 1100°C, the next series on experiments on Microstructure 2 considered forging temperatures below 1100°C. Visible grains occurred in locations between B and C (see Fig. 4, top left), although the largest ones were found in areas of effective strain between 0.1 and 0.17.

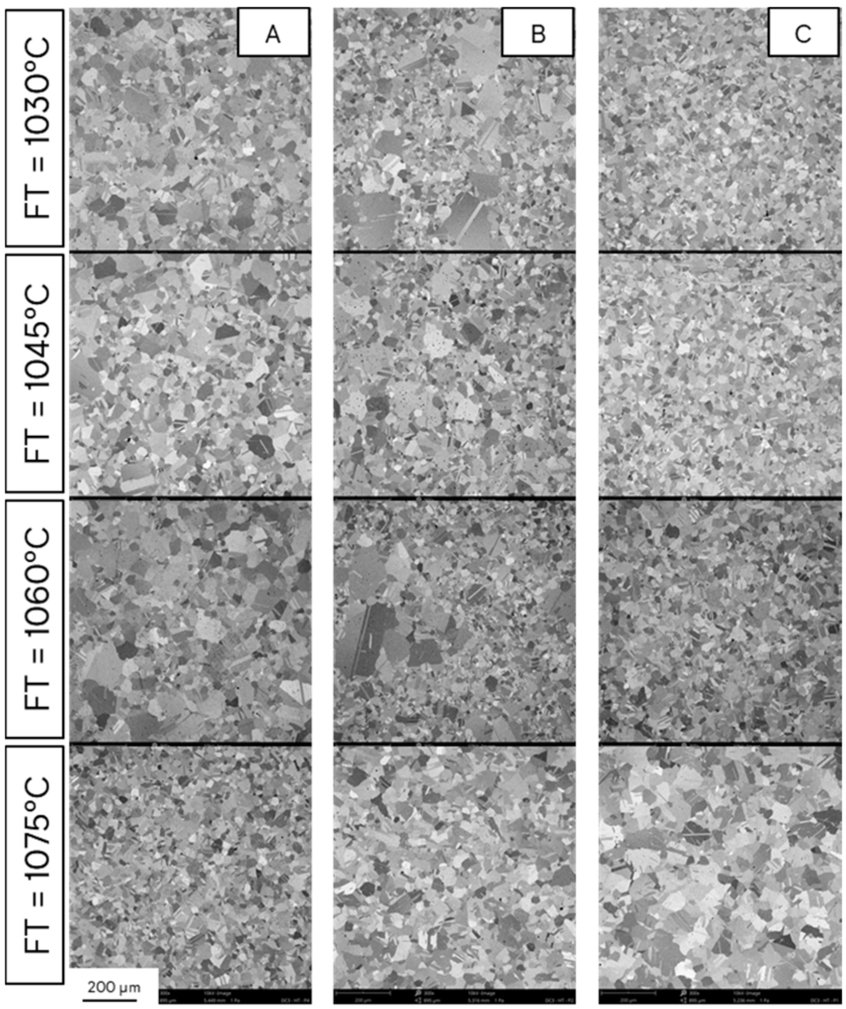

Fig.8 Backscattered electron (BSE) images (X100) for forged Microstructure 2 material after solution heat treatment (SHT) at 1185°C for 1 hour. The images show grain structures that were found at locations A, B and C (Fig. 4) in double cone test pieces forged at 1030, 1045, 1060 and 1075°C using a constant strain rate of 0.2 strain per min.

BSE images for forged Microstructure 2 material after SHT at 1185°C for 1 hour are presented in Fig. 8. The grain structure is similar across the 4 forging temperatures and 3 locations in the DC test pieces. One difference is the slightly larger average grain size in the low strain location C for the DC forged at 1075°C (Table 4). However, the grain structure does appear almost "duplex" at the other forging temperatures, with visible grains apparent, along side the smaller, average grains. These observations are consistent with the flow stress behaviour in Fig. 6, i.e. for the constant strain rate of

0.2 per min, a forging temperature of 1075°C shows little reduction in true stress with increasing true strain whereas the lower temperatures do.

Table 4 A summary of grain size in forged Microstructure 2 material after solution heat treatment (SHT) at 1185°C for 1 hour. See Fig. 4 for locations A, B and C.

Forge T (°C)	**Mean grain size (µm)**		
	A	**B**	**C**
1030	29	30	18
1045	31	33	19
1060	28	30	20
1075	18	20	36

At location D in DC test pieces, a small area is subject to a spike in maximum instantaneous strain rate at the end of the forging process. For forging at a constant strain rate of 0.2 strain per min., the predicted strain rate can be as high as 0.0155 (Fig. 4, top right). The higher strain rate produces a localised area of visible grains for forging temperatures of 1030, 1045, 1060 and 1075°C. Examples are provided in Fig. 9 for forging temperatures of 1045 and 1075°C. The location of visible grains coincides with the small area of high strain rates. However, at a higher forging temperature of 1090°C, visible grains were not found at location D although an increase in average grain was evident (Fig. 9, right).

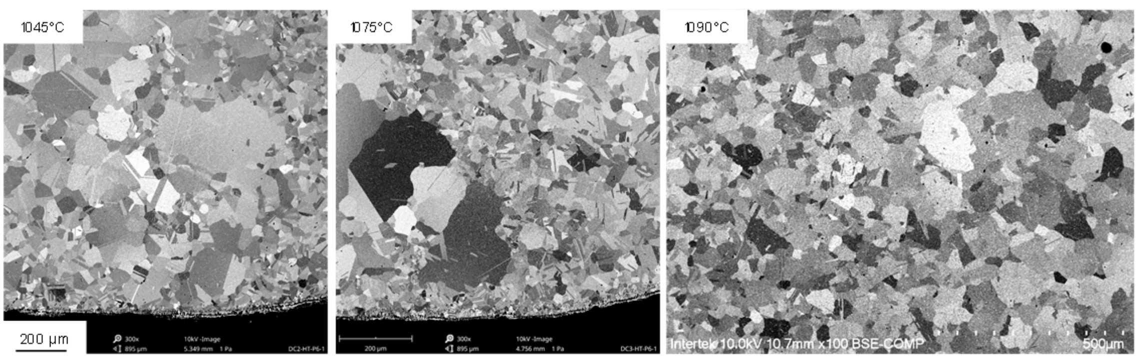

Fig. 9 Backscattered electron (BSE) images for forged Microstructure 2 material after solution heat treatment (SHT) at 1185°C for 1 hour. The images show grain structures that were found at location D (Fig. 4) in double cone (DC) test pieces forged at 1045°C (left), 1075°C (centre) and 1090°C (right) using a constant strain rate of 0.2 strain per min.

As stated earlier, DC test pieces were also forged at 0.05 and 0.5 strain per min. at 1060°C. Post SHT grain structures for Microstructure 2 material, forged at these constant strain rates, are compared with those from 0.2 strain per min in Fig. 10. Neither the average grain size in low strain, location C (top row, Fig. 10) nor the propensity for visible grains in the high strain rate area, location D (lower row, Fig. 10) appear to have changed significantly from adjusting the forging strain rate.

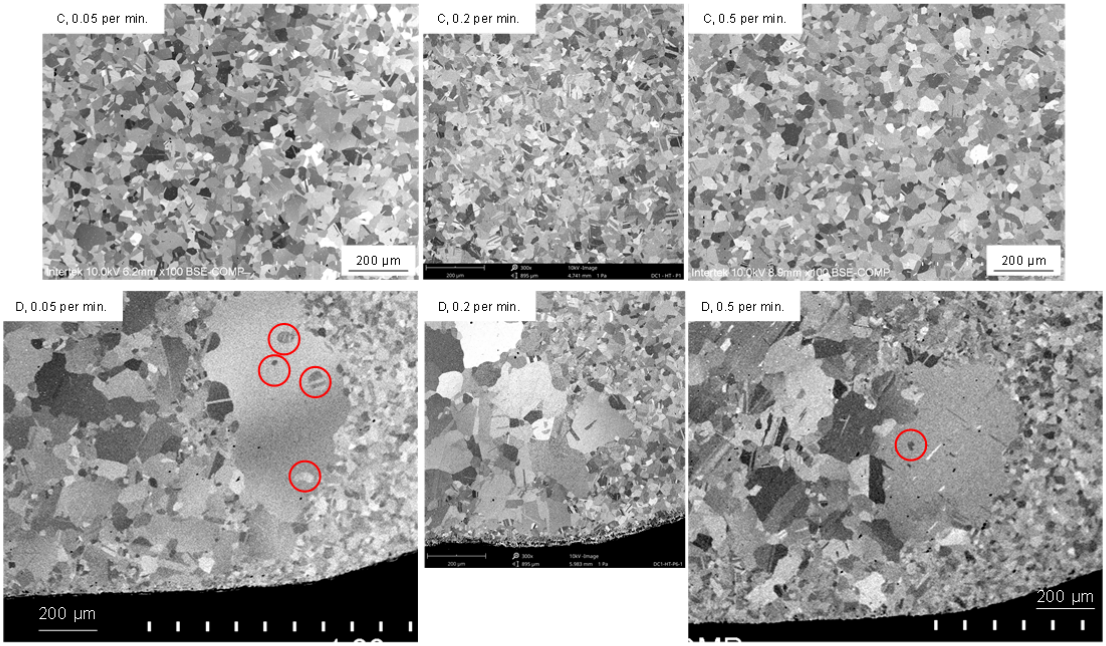

Fig. 10 Backscattered electron (BSE) images for forged Microstructure 2 material after solution heat treatment (SHT) at 1185°C for 1 hour. The images show grain structures that were found at location C (top row) and D (lower row) in double cone test pieces forged at 1060°C using a constant strain rate of 0.05 strain per min. (left), 0.2 strain per min. (centre) and 0.5 strain per min. (right). Red circles highlight isolated “normal” grains.

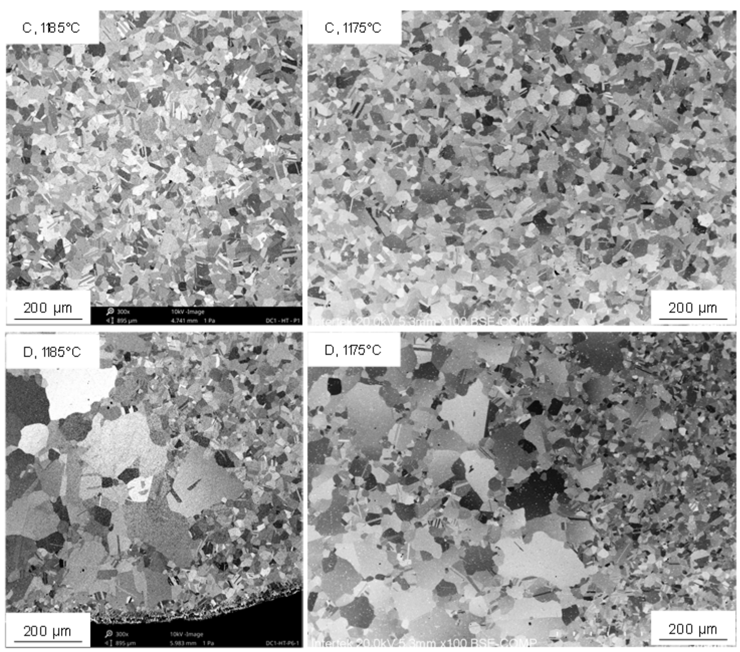

Fig. 11 Backscattered electron (BSE) images for forged Microstructure 2 material after solution heat treatment (SHT) at 1185°C (left) and 1175°C (right) for 1 hour. The images show grain structures that were found at location C (top row) and D (lower row) in double cone test pieces forged at 1060°C using a constant strain rate of 0.2 strain per min.

Whilst forging conditions has thus far been examined in this study, the effect of SHT temperature should also be considered. The majority of forged DC test pieces have received a SHT of 1185°C for 1 hour. Figure 11 compares the grain structure of Microstructure 2 material, forged at 1060°C and a constant strain rate of 0.2 strain per min., following SHT at 1185 and 1175°C. The average grain size in low strain, location C (top row, Fig. 11) does not appear to have changed significantly from reducing the SHT temperature by 10°C. However, the number density of visible grains in location D has increased marginally although the size of the largest visible grain has not changed significantly.

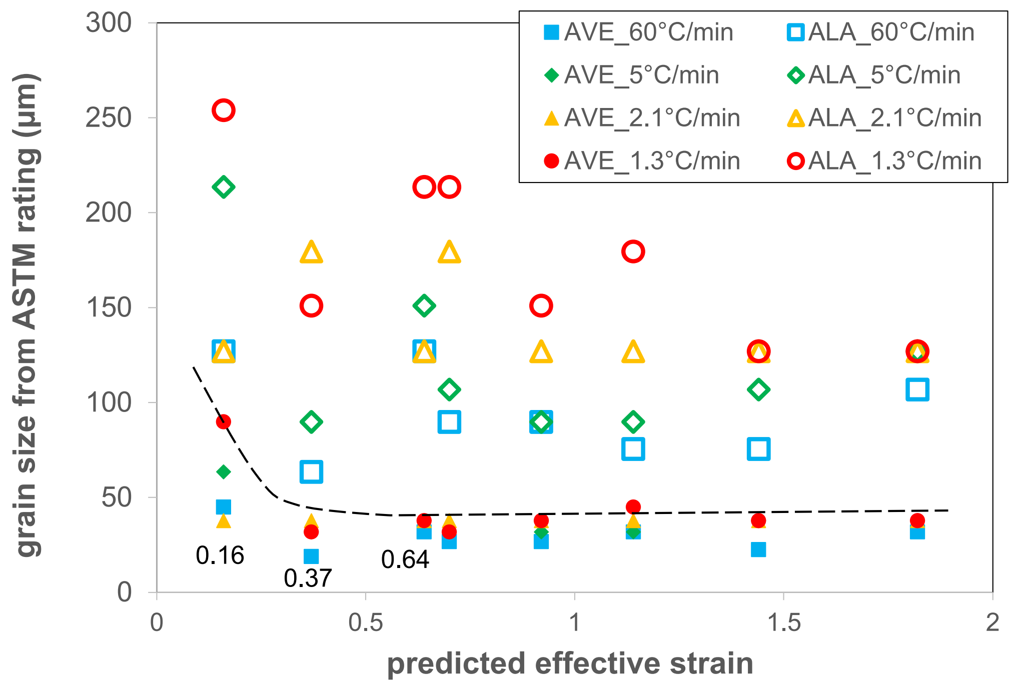

Fig. 12 Effect of forging strain and heating rate during SHT on grain size: AVE is average grain size from ASTM E112, ALA is As Large As grain size from ASTM E930. See Fig. 3 for location of samples, extracted from the centre section of a large forging (Microstructure 2). SHT was 1 hour at 1185°C.

Grain size data from samples, extracted from the centre section of a large forging (Fig. 3), after SHT are presented in Fig. 12. The SHT was 1 hour at 1185°C. The chart illustrates the effects of forging strain and heating rate during SHT on grain size. Whilst the data set does not show perfect correlations, with likely experimental variation in grain size masking trends, the general trend is for average and ALA grain size to increase with reducing forging strain and heating rates.

Discussion

The error in not soaking Microstructure 2 RCC test pieces for compression testing has offered an opportunity to examine the effects of soak time at forging temperatures on flow stress behaviour. It is evident from Fig. 7 that the flow stresses for “unsoaked” Microstructure 2 material are higher than those from the initial “soaked” Microstructure 1, despite showing a greater fraction of smaller grains. Flow stresses at these forging temperatures tend to increase with increasing grain size. Whilst Fig. 7 also showed that extending the soak time from 4 to 8 hours in Microstructure 1 material had little effect on the stress-strain behaviour, albeit with some test-to-test scatter, it is likely that secondary γ' precipitates in the starting material will coarsen and potentially dissolve during extended times at temperatures of 1030 to 1090°C. Precipitation simulations, using the mean-field approach described in [16], indicate that from an assumed heating rate of about 25-30°C/min., secondary γ' precipitates will dissolve completely before 1090°C but will still be present after 15 minutes at 1030 and 1060°C. Work has not yet been undertaken to detect the dissolution of secondary γ' precipitates during heating and thermal exposure. However, researchers from NASA [17] have reported the use of differential thermal analysis (DTA) to understand phase formation in the Low Solvus High Refractory (LSHR) alloy. Using a heating rate of 5°C/min., they showed a distinct spike in DTA heat flow data, with the peak around 1090°C, for the first heating cycle and attributed this to dissolution of secondary γ' precipitates. The onset of the spike occurred about 1075°C. As LSHR and the new alloy have similar compositions and volume fractions of γ'precipitates (51-53%), the LSHR DTA data can be extended to the new alloy, at least for the purposes of the discussion. Given that secondary γ' precipitates have a significant effect on flow stress behaviour, it is curious that there is a change in the shape of flow stress curves about 1075°C, with lower forging temperatures producing a reduction in true stress with increasing true strain and higher forging temperatures producing no or little change in true stress with increasing true strain (Fig. 6). If these precipitates do influence flow stress behaviour, along with starting grain size, do they also influence DRX? This question will not be addressed further here but is extended to the academic community for further investigation.

The compression tests on DC test pieces have identified potential forging conditions that could be used to isothermally forge large complex shapes for disc rotors. The evidence in Figs. 8-12 suggests that the ideal 20-40 μm grain size could be produced in most areas of forgings. However, particular attention should be given to areas of low forging strain and areas that are subjected to high forging strain rates as these have the potential to develop large visible grains. It should be noted that the heating rates, SHT temperature and duration that have been used in this study are possible worst cases that could exaggerate the occurrence and size of visible grains. As stated earlier, T_{solvus} for the new alloy is no higher than 1160-1165°C but grain growth could begin at slightly lower temperatures. As such, the SHT temperature could be reduced from 1185°C. This is prudent to minimise both the extent of visible grains and the propensity for quench cracks [18].

The incidence of visible grains reported in this study from low forging strain areas can be rationalised by the mechanism proposed by Bozzolo et al. [11, 12], *i.e.* that selective grain growth is due to the activation of a few nuclei that have sufficient retained strain or stored energy to exceed a critical value. Furthermore, this critical value decreases with increasing heating time for super-solvus solution heat treatment. As discussed earlier, KAM data from EBSD is a useful means of understanding levels of retained strain. Figure 13 shows KAM images from EBSD that was undertaken on 5 samples from the forging centre section (Fig. 3). The sampled area was 429 x 357 μm and the step size was 0.35 μm. It is evident from Fig. 13 that increased forging strains produce more homogeneous misorientations. The observed rotations of 1-3° in the 0 – 0.25 forging strain sample are very localised and heterogeneous, suggesting that not all grains show the same level of retained strain.

The proposed mechanism for selective grain growth can also explain the presence of visible grains at very localised areas that are subject to high strain rates. In terms of the DC test pieces, the forging strains in these small areas (Fig, 4 top left) may not be sufficiently high (0.25 – 0.5) to exceed a critical stored energy level but will create more nuclei for recrystallisation than forging strains below 0.25 (as illustrated in Fig. 13). However, the small areas in location D that receive high strain rates will show a higher number density of nuclei and a higher rate of recrystallisation than the surrounding regions that receive lower strain rates, which may trigger the development of visible grains.

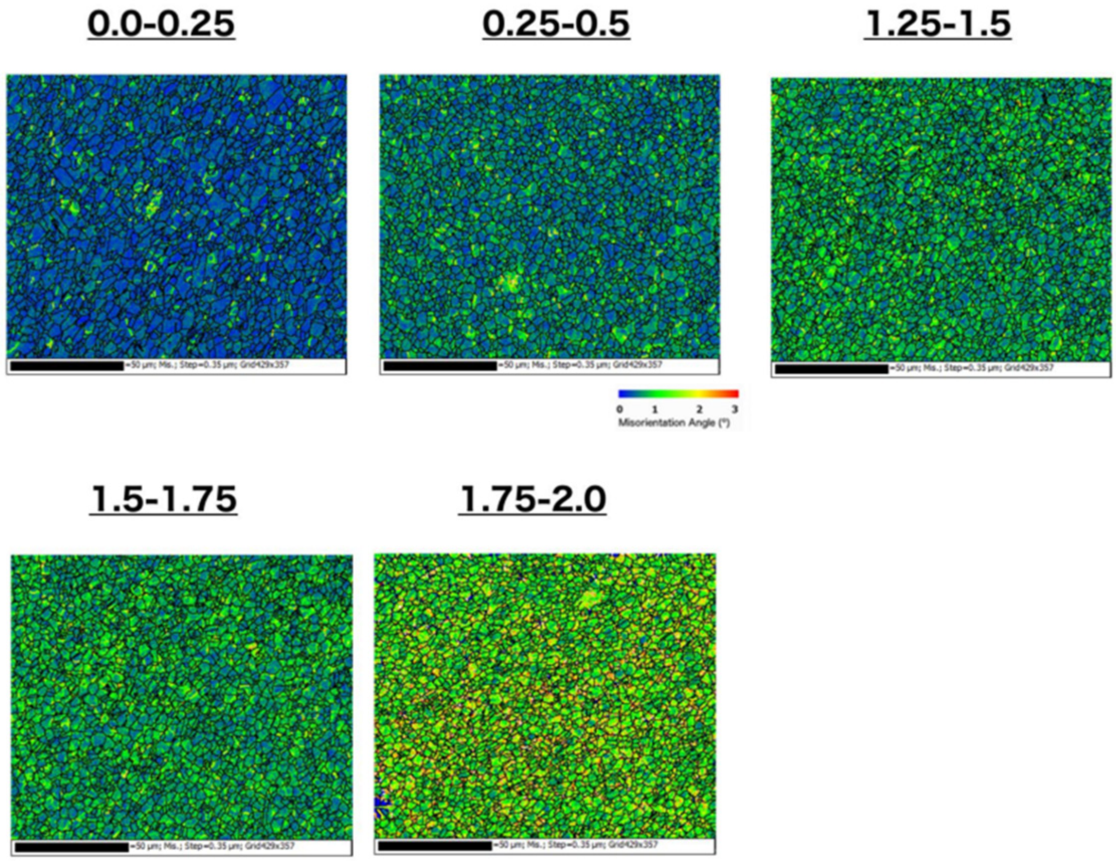

Fig. 13 Kernel Average Misorientation (KAM) images from EBSD of 5 samples in Fig. 3 in the as-forged condition. The legend indicates rotations from local misorientation of up to 3°.

Two further observations can be made from the grain structure images. The lower BSE images in Figure 10 show isolated "normal" grains within large visible grains. Examples of such occurrences are indicated by red circles. Secondly, the "normal" grains show annealing twins as expected, whereas the visible grains appear to be free of annealing twins [19]. Understanding these observations is the subject of future research.

Summary

The results of experimental work and process simulations have been presented to understand forging and heat treatment conditions that produce visible grains in a new powder Ni superalloy that has been developed for disc rotor applications. These have identified potential forging conditions that could be used to isothermally forge large complex shapes for disc rotors. The evidence presented suggests that the ideal 20-40 µm grain size could be produced in most areas of forgings. However, particular attention should be given to areas of low forging strain and areas that are subjected to high forging strain rates as these have the potential to develop large visible grains. It should be noted that the heating rates, solution heat treatment temperature and duration that have been used in this study are possible worst cases that could exaggerate the occurrence and size of visible grains. The incidence of visible grains reported in this study from low forging strain areas can be rationalised by the mechanism proposed by Bozzolo et al., *i.e.* that selective grain growth is due to the activation of a few nuclei that have sufficient retained strain or stored energy to exceed a critical value. Furthermore, this critical value decreases with increasing heating time for super-solvus solution heat treatment.

It is recommended that caution should be exercised in using laboratory compression test pieces and heat treatment trials to simulate conditions in full-scale forgings. Wherever possible, relevant starting materials/microstructures, soak times and heating rates for industrial forgings should be used for laboratory test pieces to ensure that the data and information that are generated are representative.

Acknowledgements

This work was supported by Rolls-Royce plc and the Innovate-UK UHTNA and CRUISE projects. Drs Hardy and Buckingham would like to thank Rolls-Royce colleague Dr Han Tai for his support and encouragement in this work, Paul Wesseling of Rolls-Royce Corporation for his support, Cameron Brett, Zak Lomas of Rolls-Royce, Andrew Wilkinson and Stuart White of Intertek Derby for sample preparation and electron microscopy.

Conflict of Interest Statement

On behalf of all authors, the corresponding author states that there is no conflict of interest.

References

1. **Online document:** P. Argüelles, J. Lumsden, M. Bischoff, D. Ranque, P. Busquin, S. Rasmussen, B.A.C. Droste, P. Reutlinger, R. Evans, R. Robins, W. Kröll, H. Terho, J.-L. Lagardère, A. Wittlöv and A. Lina: European Aeronautics: A Vision for 2020 (Advisory Council for Aviation Research and Innovation in Europe), https://op.europa.eu/en/publication-detail/-/publication/214b7682-3947-411f-bcb5-92cb03ea7931. Accessed 13 August 2022.
2. **Online document:** M. Darecki, C. Edelstenne, T. Enders, E. Fernandez, P. Hartman, J.-P. Herteman, M. Kerkloh, I. King, P. Ky, M. Mathieu, G. Orsi, G. Schotman, C. Smith and J.-D. Worner: Flightpath 2050 Europe's vision for aviation (European Commission), https://op.europa.eu/en/publication-detail/-/publication/7d834950-1f5e-480f-ab70-ab96e4a0a0a. Accessed 13 August 2022.
3. R.C. Reed, A. Mottura and D.J. Crudden: *Superalloys 2016*, M. Hardy, E. Huron, U. Glatzel, B. Griffin, B. Lewis, C. Rae, V. Seetharaman and S. Tin, eds., TMS, Warrendale, PA, USA, 2016, pp. 15-23.
4. R.J. Mitchell, J.A. Lemsky, R. Ramanathan, H.Y. Li, K.M. Perkins and L.D. Connor: *Superalloys 2008*, R.C. Reed, K.A. Green, P. Caron, T. Gabb, M.G. Fahrmann, E.S. Huron and S.A. Woodard, eds., TMS, Warrendale, PA, USA, 2008, pp. 347-356.
5. **Online document:** D. Anderson: Fuel Conservation Operational Procedures for Environmental Performance (International Civil Aviation Organisation) https://www.icao.int/Meetings/EnvironmentalWorkshops/Documents/ICAO-TransportCanada-2006/Anderson_ops.pdf. Accessed 13 August 2022.
6. M.C. Hardy, C. Argyrakis, H. S. Kitaguchi, A. S. Wilson, R. C. Buckingham, K. Severs, S. Yu, C. Jackson, E. J. Pickering, S. C. H. Llewelyn, C. Papadaki, K. A. Christofidou, P. M. Mignanelli, A.

Evans, D. J. Child, H. Y. Li, N. G. Jones, C. M. F. Rae, P. Bowen, and H. J. Stone: *Superalloys 2020*, S. Tin, M. Hardy, J. Clews, J. Cormier, Q. Feng, J. Marcin, C. O'Brien and A. Suzuki, eds., The Minerals, Metals & Materials Series, Warrendale, PA, USA, 2020, pp. 19-30. https://doi.org/10.1007/978-3-030-51834-9_2.

7. R.L. Dreshfield and H.R. Gray: *P/M Superalloys – a Troubled Adolescent*, NASA Technical Memorandum, TM-83623, Lewis Research Center, Cleveland, Ohio, USA, June 1984.
8. R. Anderson: *The International Journal of Powder Metallurgy*, 1990, vol. 26, (2), pp. 171-178.
9. J. Smythe: *Advanced Materials and Processes*, 2008, November, pp. 52-55. https://www.asminternational.org/documents/10192/1887146/amp16611p052.pdf/6664af73-fa87-4c2f-8b94-d420d5c438e3/AMP16611P052. Accessed 13 August 2022.
10. M.C. Hardy, M. Detrois, E.T. McDevitt, C. Argyrakis, V. Saraf, P.D. Jablonski, J.A. Hawk, R.C. Buckingham, H.S. Kitaguchi and S. Tin: *Metall. Mater. Trans. A*, 2020, vol. 51A (6), pp. 2626-2650.
11. N. Bozzolo, A. Agnoli, N. Souai, M. Bernacki and R.E. Loge: *5th International Conference on Recrystallization and Grain Growth*, Sydney, Australia, 2013, DOI: 10.4028/www.scientific.net/MSF.753.321.
12. A. Agnoli, M. Bernacki, R. Logé, J-M. Franchet, J. Laigo and N. Bozzolo: *Metall. Mater. Trans. A*, 2015, vol. 46A (9), pp. 4405-4421.
13. V.M. Miller, A.E. Johnson, C.J. Torbet, and T.M. Pollock: *Metall. Mater. Trans. A*, 2016, vol. 47A (4), pp. 1566-1574.
14. M.C. Hardy, R.C. Reed, D. Crudden, United States Patent US 10,422,024 B2, 24 September 2019
15. G.J. Davies, J.W. Edington, C.P. Cutler and K.A. Padmanabhan: *Journal of Materials Science*, 1970, vol. 5 (12), pp. 1091-1102.
16. M.J. Anderson, F. Schulz, Y. Lu, H.S. Kitaguchi, P. Bowen, C. Argyrakis and H.C. Basoalto: *Acta Mater.*, 2020, vol. 191, pp. 81-100.
17. T.P. Gabb, A. Garg, D.R. Miller, C.K. Sudbrack, D.R. Hull, D. Johnson, R.B. Rogers, J. Gayda and S.L. Semiatin, *Formation of Minor Phases in a Nickel-Based Disk Superalloy*, NASA Technical Memorandum TM-2012-217604, Glenn Research Center, Cleveland, Ohio, USA, 2012.
18. J. Gayda, P. Kantzos and J. Miller, *Quench Crack Behavior of Nickel-Base Disk Superalloys*, NASA/TM-2002-211994, NASA Technical Memorandum TM-2002-211984, Glenn Research Center, Cleveland, Ohio, USA, 2002.
19. N. Bozzolo, (2022), Private Communication, MINES ParisTech, France.